IBRACON Structures and Materials Journal
Revista IBRACON de Estruturas e Materiais

ORIGINAL ARTICLE

Determination of coarse aggregate content of concrete specimens by wave propagation and Artificial Neural Network

Determinação do teor de agregado graúdo em amostras de concreto por propagação de ondas e Redes Neurais Artificiais

Danilo Pereira dos Santos[a] (ID)
Vladimir Guilherme Haach[b] (ID)

[a]Instituto Federal de Educação, Ciência e Tecnologia da Bahia, Vitória da Conquista, BA, Brasil
[b]Universidade de São Paulo, Escola de Engenharia de São Carlos, São Carlos, SP, Brasil

Abstract: Nondestructive tests that assess the constitution or degradation of structures are of great interest in Civil Engineering. Among the non-destructive testing techniques, the Ultrasonic Pulse Velocity (UPV) test stands out; however, although its use is widespread, there are still no applications that employ this method to determine the constitution of concrete *in situ*. Therefore, this article addresses the identification of the coarse aggregate content in concrete specimens by an Artificial Neural Network (ANN) trained with a database of numerical tests that simulated UPV. In this paper, the coarse aggregate content will be described as a percentage of the total area of a two-dimensional concrete model. Three artificial neural network architectures were evaluated. The first two, trained with 13 or 22 paths, solved a classification problem for five aggregate contents, and the third, trained with 22 paths, solved a regression problem. Its performance was compared with those of other regression solutions, namely XGB Regressor, Random Forest, and OLS (Ordinary Least Squares), and showed superior, with -2.55% to +2.17% average deviations. Thus, this paper demonstrated that the use of ANN in combination with UPV test has the potential to identify the coarse aggregate content in concretes. The positive results suggest that this approach is promising and highlights the need for further experimental validation in future research.

Keywords: nondestructive test, ultrasonic pulse velocity, concrete, machine learning.

Resumo: Ensaios não destrutivos (END) que avaliam a constituição ou degradação de estruturas são de grande interesse na Engenharia Civil. Entre as técnicas de END, destaca-se o teste de Velocidade de Pulso Ultrassônico (UPV); no entanto, embora seu uso seja difundido, ainda não existem aplicações que empreguem esse método para determinar a constituição do concreto *in situ*. Portanto, este artigo aborda a identificação do teor de agregados graúdos em amostras de concreto por meio de uma Rede Neural Artificial (RNA) treinada com um banco de dados de ensaios numéricos que simularam UPV. Neste artigo, o teor de agregados graúdos será descrito como uma porcentagem da área total de um modelo bidimensional de concreto. Três arquiteturas de redes neurais artificiais foram avaliadas. As duas primeiras, treinadas com 13 ou 22 trajetórias, resolveram um problema de classificação para cinco teores de agregados, e a terceira, treinada com 22 trajetórias, resolveu um problema de regressão. Seu desempenho foi comparado com o de outras soluções de regressão, a saber, Regressor XGB, Random Forest e Mínimos Quadrados Ordinários, e mostrou-se superior, com desvios médios de -2,55% a +2,17%. Assim, este artigo demonstrou que o uso da RNA em combinação com o teste UPV tem o potencial de identificar o teor de agregados graúdos em concretos. Os resultados positivos sugerem que essa abordagem é promissora e ressaltam a necessidade de validação experimental adicional em pesquisas futuras.

Palavras-chave: teste não destrutivo, velocidade de pulso ultrassônico, concreto, aprendizagem de máquina.

1 INTRODUCTION

According to Dhillon [1], the term *life cycle costing* was used in 1965 for the first time and represents all costs incurred during the life span of a system. After more than half a century, this definition continues to gain prominence. The different disciplines that support the construction industry should optimize those costs, thus, effectively contributing to a sustainable society. The American Concrete Institute (ACI) estimates that 18 to 21 billion dollars are spent on repairs every year in the USA [2]; therefore, techniques that assess structural degradation or material characterization are essential for the optimization of such resources.

As will be presented, the interest in developing techniques that assess the concrete structures without extracting a specimen has grown; but, the methods for determining concrete constitution from these nondestructive tests are still scarce. The UPV is a relevant technique in assessing structural health; therefore, this work aims to evaluate the possibility for the UPV test also to be suitable for determining the coarse aggregate content in concrete structures.

Traditionally the UPV has been widely used for investigating concrete structures (e.g., study of the mechanical properties of concrete in early ages [3]–[5], water/cement (w/c) determination [6]–[8], damage identification in large structures and concrete specimens [9], [10], identification of grout filling [11], [12], evaluation of stress state [13]–[16] and tomography generations [17]–[23]. It is also possible to find papers that correlate the UPV to the compressive strength of simple or high permeability concretes [24], [25]. Recycled aggregate concretes and special mortars were also evaluated for their porosity and strength characteristics through UPV tests [26]–[29]. Finally, UPV tests are also applied to assess the integrity of other materials in Civil Engineering, such as wood and masonry buildings [30]–[34].

However, despite the varied applications of UPV, the authors have not found any study that uses this technique to determine the composition of a concrete mix *in situ*. Therefore, this work aims to fill this gap by presenting a methodology that estimates the coarse aggregate content in a concrete specimen.

The correlation between the coarse aggregate content and the ultrasonic pulse velocity is highly non-linear since an infinite number of distributions is possible for each aggregate content.

In the literature, there are established options for solving nonlinear problems (e.g., Powell's Method, BFGS, and bio-inspired algorithms). In this context, the present authors sought applications similar to the proposal presented in this paper. It was observed that solutions using artificial neural networks for problems with UPV pulse input data were positive [35]–[41].

Thus, the present study investigated the use of wave propagation and ANN for determining the coarse aggregate content of concrete specimens. Numerical tests based on the wave propagation theory were conducted in a continuous homogeneous and isotropic medium, and were the database for training an ANN for identifying such content.

As discussed, ANNs have been widely applied in nondestructive tests. Shah et al. [42] used them to estimate the degradation level of concrete specimens, and reported a two-layer-perceptrons network provides a good fit. The ANN employed was trained with the time-domain signals of ultrasonic waves obtained in experimental tests, and successfully predicted the residual strength of other concrete specimens.

Xu and Jin [43] used UPV to train an artificial neural network for identifying RC corrosion. The authors employed 50 specimens as a database for the training, and observed the Radial Basis Function-based model was more efficient than the Back Propagation-based one for training the ANN. The input parameters of the network included the UPV, the specimen geometry, and the concrete strength. Despite the small number of geometries, the neural network combined with the UPV showed good performance in identifying corrosion in RC.

The strength of Lightweight aggregate concrete (LWAC) may be affected by segregation. Tenza-Abril et al. [44] used ANN to predict strength through ultrasonic pulse in LWAC specimens. A six-neuron neural network hidden layer architecture was chosen, and seven input data were supplied to the ANN, including the UPV and the aggregate density. The results showed ANN associated with ultrasonic pulse velocity can be useful for studies of LWAC segregation and its strength.

ANNs have also been used for assessments of fresh concrete. Jain et al. [45] studied the relationship between concrete slump and concrete mix constituents, and the most complex ANN analyzed considered water, cement, coarse aggregates, and sand content as inputs. The results showed ANN was able to predict concrete slumps with higher precision than the other regression methods studied.

Ghafari et al. [46] applied ANN for the study of UHPC composition. The network was built with 15 neurons in the hidden layer and received the proportion of cement, sand, silica fume, quartz flour, water superplasticizer, and steel fiber as input data. It was trained by 53 different mixtures and showed good predictions for compressive strength and slump flow. Such accuracy was verified in additional experimental tests.

As informed, the authors did not find studies that applied UPV in identifying the constitution of concrete; however, other researchers have investigated the concrete constitution using electromagnetic (EM) wave propagation and the

dielectric properties of concrete. Soutsos et al. [47] applied radar testing to assess concretes with pulverized fuel ash (PFA), ground granulated blast furnace slag (GGBS), steel fibers, and honeycombing due to poor compaction. The authors observed less influence exerted by constituents and strength in comparison to moisture. The exceptions were honeycombing and steel fibers, since they significantly affected conductivity.

Dérobert and Villain [48] proposed a multi-linear polynomial relationship among relative permittivity and five concrete mix parameters, of which two are qualitative (aggregate and cement nature), and three are quantitative (aggregate and cement content, and w/c). The ground-penetrating radar (GPR) generated the electromagnetic wave. Under dry conditions, the influence of aggregate nature was higher, and the cement nature and w/c ratio were substantial. The generation of the multi-linear polynomial model revealed a relation between the concrete mix parameters and relative permittivity.

Villain et al. [49] studied concretes mixed with silico-calcareous aggregates and siliceous aggregates, and observed the aggregate nature influences both dielectric constant and complex permittivity, thus establishing a relationship between them with w/c. They studied six concretes and found linear correlations for such properties.

Microwaves were used in some studies to identify the constitution of the concrete mix. Bois et al. [50] employed an open-ended rectangular waveguide (OERW) in their analysis, and two w/c and two coarse aggregate-to-cement (ca/c) ratios were evaluated by six concrete specimens. Measurements at 3 GHz indicated a relationship between w/c and the magnitude of the reflection coefficient. The authors also observed ca/c could be correlated to the standard deviation of the reflection coefficient magnitude at 10 GHz.

Investigating the mechanical strength of concrete structures is a primary focus of research in this field, and significant progress has been made in this area. However, durability is not only determined by mechanical strength but is also influenced by other factors. For example, previous researches have shown that the content of coarse aggregates can significantly impact the durability of concrete under abrasive conditions [51]. While mechanical strength remains an important factor for durability, it is crucial to develop technologies that go beyond estimating strength in order to achieve greater durability in concrete constructions.

It should be highlighted that determining the proportions present in a concrete mixture through the propagation of mechanical waves is a challenge. Thus, as a first approach, the authors decided to demonstrate a methodology for identifying the portion responsible for the greatest heterogeneity of undamaged concrete, i.e., the coarse aggregates.

Therefore, the present study aims to contribute to the nondestructive test field, offering an alternative that combines a UPV test and an artificial neural network to identify the coarse aggregate contents of a concrete specimen.

2 ASSESSMENT OF COARSE AGGREGATE CONTENT THROUGH UPV-ANN ASSOCIATION

The test based on ultrasonic pulse velocity measures the travel time of an ultrasonic pulse in a continuous medium [52]. The Theory of Elasticity enables relations between wave velocities and mechanical properties, calculated by Equations 1 and 2 for P-waves (c_p) and S-waves (c_s), respectively, for isotropic and homogeneous media.

$$c_p = \sqrt{\frac{\lambda + 2G}{\rho}} \tag{1}$$

$$c_s = \sqrt{\frac{G}{\rho}} \tag{2}$$

where G, λ and ρ are shear modulus, Lamé's first parameter, and material density, respectively.

The ultrasonic pulse theoretically travels on a straight path if a continuous, linear, homogeneous, and isotropic medium is assumed. Any discontinuity or heterogeneity in the medium, such as voids, cracks, or particles of a different material leads to changes in the travel paths, which depend on the velocity medium.

Figure 1 shows six transducers and thirteen possible paths between them. The travel-time associated with any path is easily calculated, since the wave velocity in the uniform medium is known. On the other hand, Figure 1b displays a heterogeneity that modifies the travel-time between transducers 1-3 and 2-6.
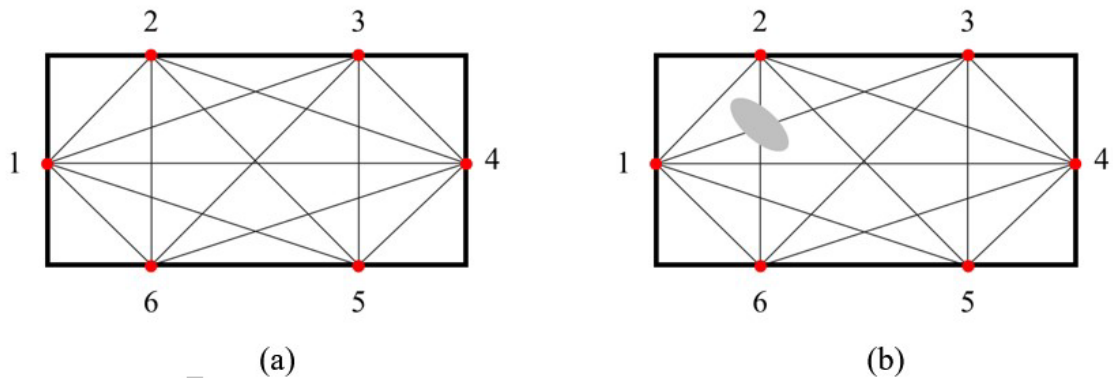
Figure 1. Influence of heterogeneities on the travel-times of ultrasonic pulses.

Therefore, a relationship can be established between travel-times and heterogeneity content. For structural concrete applications, assuming an isotropic mortar and undamaged specimen, the heterogeneities are the coarse aggregates.

However, specimens with the same coarse aggregate content may have different travel-times affected by heterogeneities, since the coarse aggregate distribution is random. The present study employed several distributions for each content in the ANN training algorithm, so that the neural networks trained for different coarse aggregate distributions would identify the coarse aggregate content of specimens through an ultrasonic pulse velocity test.

The study was conducted using two-dimensional numerical models, representing a cross-section of 100 x 200 mm^2 with up to 391.87 mm^2 of aggregates. Figure 2 shows an example of the geometry.
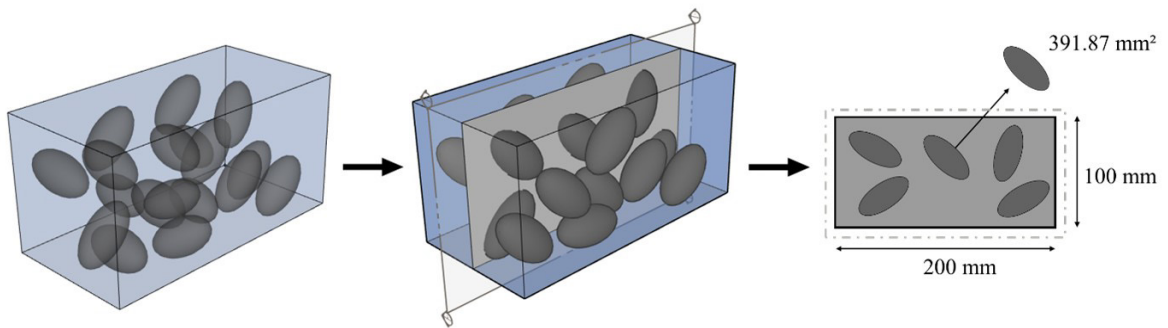

Figure 2. Concept of the adopted geometry.

The coarse aggregate content (CaC) was defined as the ratio between aggregates area (A_{ag}) and non-aggregates area, Equation 3, where n is the number of aggregates and A_{cs} is the cross-section area.

$$CaC = \frac{A_{ag} \cdot n}{A_{cs} - A_{ag} \cdot n} \tag{3}$$

It should be noted that the CaC definition established in this paper does not correspond to the actual proportion of a concrete mixture, which is described in terms of volume. This limitation arises due to the two-dimensional nature of the study conducted in this research.

As detailed in the following sections, a large dataset was generated. This dataset was formed with pulse travel times from different measurement sets. Each measurement set, constituting a sample, was generated by varying the coarse aggregate content (CaC), aggregate positions (x, y), and relative rotation of the aggregates.

Figure 3 depicts the position of the aggregate and its rotated local axes. It's worth noting that the algorithm does not allow the superposition of aggregates.
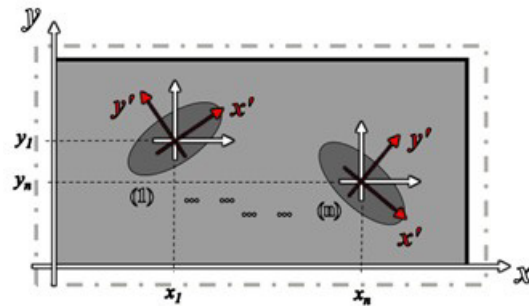

Figure 3. Geometric variables: aggregate Positions and rotated local axes

The P-wave velocities assigned to the mortar and to the coarse aggregate (basaltic) were 3013 m/s and 5645 m/s, respectively [53], [54].

2.1 General criteria applied in neural network construction

The fundamental component of a neural network is the artificial neuron. There is a well-established graphical representation in the literature, depicted in Figure 4.
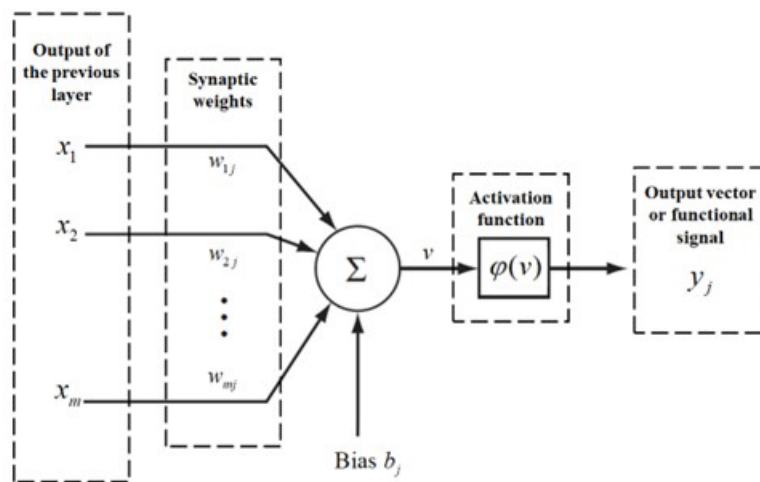
Figure 4. Artificial neuron: basic architecture.

The processing carried out by a neuron involves receiving a vector from the preceding layers, multiplying these components by a set of weights (*w*), and summing them while adding the bias value (if applicable). Thus, these operations can be represented by Equation 4.

$$v = \sum_{i=1}^{m} w_i x_i + bias \tag{4}$$

The induced local field (Equation 4) undergoes an activation function that produces the final output of that neuron.

Rev. IBRACON Estrut. Mater., vol. 17, no. 6, e17612, 2024

5/21

Several activation functions are available for use in neural networks, and their selection depends on the desired outcome. The activation functions used in this paper were:

- Rectified Linear Unit (*ReLU*): This is a discontinuous linear function that returns zero for any non-positive response. This activation function is common in convolutional neural networks, attesting to its effectiveness in deep learning problems. While *ReLU* is a non-linear function, it preserves linear function properties in terms of optimization. Due to this characteristic, *ReLU* was employed in the hidden layers of the tested architectures.
- *Linear*: The *Linear* activation function is alternatively known as "identity" (as it multiplies the input by 1.0). Thus, the *Linear* activation function preserves the weighted sum of the input.

The inclusion of this function in the classification architectures was driven by numerical considerations; tests confirmed that its presence in the penultimate layer enhanced the results of the output layer. As for the regression-dedicated architecture, this function was adopted in the final layer.

- *Softmax*: This function is frequently used in the output layers of multilayer problems. Its main objective is to allocate the probability that each value in the output vector signifies the correct answer to the problem. Given that the output labels in all the analyzed classification cases were easily identifiable (coarse aggregate content), *Softmax* was chosen.

It is worth mentioning that in the initial analyses, the S*igmoid* function and *Hyperbolic Tangent* were evaluated for the hidden layers. However, this approach was abandoned as the *ReLU* function yielded good results with simplicity.

The network model applied in this paper was the *feedforward* multilayer, meaning the network was built with an input layer, a certain number of hidden layers, and an output layer. Thus, the information flows through the network in a unidirectional manner, from the input layer towards the output layer. In other words, the output of a neuron cannot be used as input for neurons in earlier layers.

The architectures evaluated for this study initially aimed to meet heuristics that correlated the number of input vectors, output vectors, and hidden layers. However, numerous modifications were made during the process, such that the final results no longer adhered to the initial standards.

Therefore, although it may not represent the most optimal strategy, the authors systematically examined various parameters, including hidden layers and number of neurons. The outcomes provided insights into elements that should either be retained or improved. In cases where an improved parameter, despite incurring higher computational costs, did not yield substantial advantages, we chose to discard that modification.

In anticipation of future experimental analyses, the number of measured paths varied in this paper between 13 and 22 paths. This initial characteristic determines the number of neurons in the first layer (as will be discussed in section 2.2).

In the process of hyperparameter tuning, the first network that provided good results for the problem with 13 inputs was the one with 22 hidden layers. The initial analyses were conducted with a lower number of neurons and hidden layers, and the results consistently improved up to the number of 22 layers. Beyond this value, no significant gains were observed.

For the problem with 22 paths, we found that instead of increasing the number of hidden layers, increasing the number of neurons per layer would achieve the desired accuracy for this new architecture.

The format of the input data for the neural networks was the same for all studied cases. Each sample (whether from the test or training dataset) was represented as a row in a matrix. The columns of this matrix contained information such as "ID Path / Transmitter Point / Receiver Point / Travel Time." The total number of rows in the matrix corresponded to the number of samples.

Therefore, for the "13 paths" ANN (section 2.2.1), the input layer processed groups of thirteen rows of the matrices intended for them. Similarly, the "22 paths" ANNs (sections 2.2.2 and 2.2.3) utilized sequences of 22 rows of the matrices generated for this case.

After applying the *Softmax* function for activation, the output layer consistently produced responses in the same format across all cases. This output conveyed the probability that the label associated with the aggregate content represented the correct answer.

After defining the network architecture, the next step involves addressing the training process. In this study, we utilized a supervised learning approach, wherein the training dataset was known both in its input and output. This configuration allows the network's error to be immediately evaluated and used to adjust its weights.

The *backpropagation* algorithm stands out as one of the most commonly employed supervised learning techniques. In this iterative process, the network is initially presented with input data, generating an output based on the current set of weights. Discrepancies between this output and the desired target values result in an error, which is subsequently *backpropagated* through the network.

This *backpropagation* process serves to adjust the synaptic weights, refining the network's performance over successive iterations. Each complete training set is referred to as an epoch of training. Therefore, after each *n*-epoch of

training, there is a set of weights $w_{ij}(n)$, corresponding to the output of neuron i and the input of neuron j. The correction applied in each iteration is denoted by $\Delta w_{ij}(n)$ and is represented by Equation 5.

$$\Delta w_{ij}(n) = \eta \delta_j(n) y_j(n) \tag{5}$$

The value of η corresponds to the learning rate of the algorithm. Although it is possible to assign various values to η, the authors have opted to fix its value at 0.01.

As depicted in Figure 4, $y_j(n)$ represents the outcome of the activation function applied to the induced field during training epoch n. In other words:

$$y_j(n) = \varphi(v_j(n)) \tag{6}$$

The $\delta_i(n)$ (Equation 5) represents the local gradient, and its calculation depends on determining a total error energy function, Equation 7.

$$E(n) = \frac{1}{2} \sum_j e_j^2(n) \tag{7}$$

Let's consider e_j as the error signal linked to each neuron j, which will be presented in Section 2.2. Thus, the local gradient can be expressed in the form of Equation 8.

$$\begin{aligned}
\delta_j(n) &= -\frac{\partial E(n)}{\partial v_j(n)} \\
&= -\frac{\partial E(n)}{\partial e_j(n)} \frac{\partial e(n)}{\partial y_j(n)} \frac{\partial y(n)}{\partial v_j(n)}
\end{aligned} \tag{8}$$

Therefore, once a differentiable activation function is defined, all the quantities are determined. The functions associated with each neural network will be detailed in the next section.

2.2 Architectures of the ANNs

Three architectures of artificial neural networks were studied, and two measurement configurations of the UPV were assessed. The first configuration used 13 measurement paths, and the second used 22 (see Figure 5).
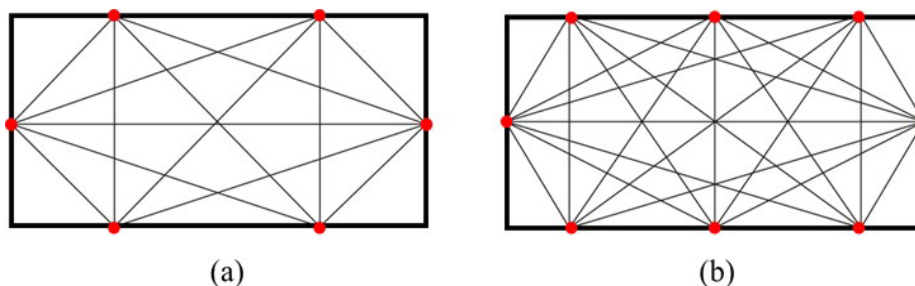

Figure 5. Measurements configurations in 100 x 200 m^2 specimens: (a) 13 paths, (b) 22 paths.

Rev. IBRACON Estrut. Mater., vol. 17, no. 6, e17612, 2024

7/21

The performance of the network was evaluated for classification and regression problems. Below are the three ANN architectures:

(i)   ANN 1 (13 paths): classification problem.

(ii) ANN 2 (22 paths): classification problem.

(iii) ANN 3 (22 paths): regression problem.

The number of neurons in the input layer was equal to the number of measurement paths for all ANN architectures. The following sections provide details of the ANNs.

2.2.1 Architecture of ANN 1

Five content labels (10.9%, 21.4%, 30.7%, 41.6% and 49.9%) were defined for the classification problem. **Table 1** shows the relationship between the number of particles and the coarse aggregate content.

Table 1. Coarse aggregate contents for the classification problems.

Specimen area (mm²)	Coarse aggregate area (mm²)	Number of coarse aggregates	Coarse aggregate contents (%)
		5	10.9
		9	21.4
20000	391.87	12	30.7
		15	41.6
		17	49.9

Five neurons were set in the output layer with the *Softmax* activation function, mathematically represented by Equation 9. *Softmax* is commonly used for classification problems as its output provides the probability of correctness for each neuron's classification.

$$\phi_i = \frac{e^{x_i}}{\sum_{j=1}^{k} e^{x_j}}$$

(9)

where i is the index representing the neuron, k is the total number of neurons in the output layer, and x is the value in the neuron before applying the *Softmax* function.

Twelve hidden layers with 26 neurons each were used, and the *ReLU* activation function was applied. An exception was the last hidden layer, which used *Linear* activation function.

The *ReLU* function updates the value of x that arrives at the neuron according to the definition of Equation 10, i.e., it returns zero for any negative x value and the value itself otherwise.

$$\phi_i = \max\left(0, x_i\right)$$

(10)

Figure 6 displays the network architecture.

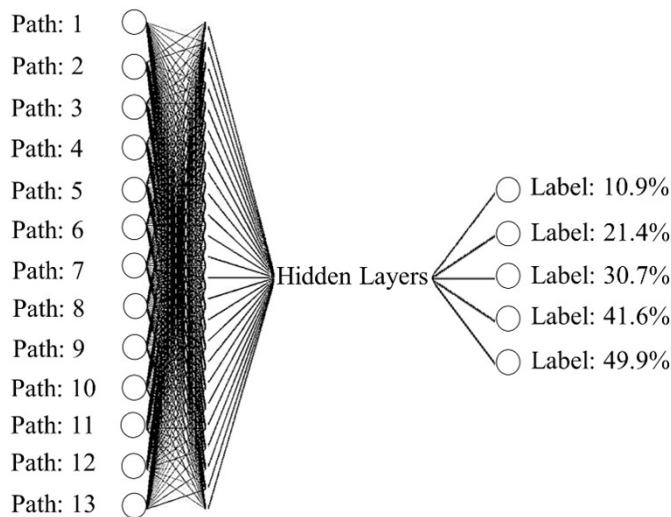Rev. IBRACON Estrut. Mater., vol. 17, no. 6, e17612, 2024

8/21

Figure 6. Architecture of ANN 1.

Categorical cross-entropy was used as the objective function, Equation 11, for the network training. It computes the losses between the target value (y_i) and the model output (y_i*), and N is the output size. The optimization was performed by *Adam* algorithm [55], available in the Tensorflow® library.

$$L(y_i, y_i^*) = -\sum_{i=0}^{N} y_i \log(y_i^*)$$ (11)

The neurons in the output layer provide values between 0 and 1. Therefore, *Softmax* ensures the sum of the results is 1. Contents different from those specified in the labels can be obtained through a weighted average of the network's response.

The coarse aggregates for each of the five content labels were randomly varied 1000 times, resulting in 5000 samples for the ANN training. This random selection affects the *(x,y)* positioning of the aggregate and its rotation angle. Additionally, the algorithm does not allow aggregate geometries to overlap or extend beyond the boundaries of the specimen. Therefore, these specimens had different locations and orientations in order to bring generality to the samples.

As explained, this neural network solves a classification problem, consequently, the chosen quality metric is Accuracy. This means we are interested in knowing how many times the neural network was able to correctly classify the expected result.

The network's training was evaluated with 100 new samples, i.e., 20 for each content. Table 2 shows the accuracy results.

Table 2. ANN 1 training evaluation.

Epochs	Accuracy (%)
10	56
100	71
1000	67
2000	77
3000	74

Therefore, 2000 training epochs were set as an optimal number for ANN 1.

2.2.2 Architecture of ANN 2

The basic difference between ANN 1 and ANN 2 is the number of neurons and layers, since both activation functions and optimization algorithm employed were the same.

The neural network was implemented with 22 neurons in the input layer and 12 hidden layers with 44 neurons in each layer. *ReLU* was used for all hidden layers, except the last, for which the *Linear* function was adopted. The output layer consisted of five neurons with *Softmax* activation function. Figure 7 illustrates the network architecture.
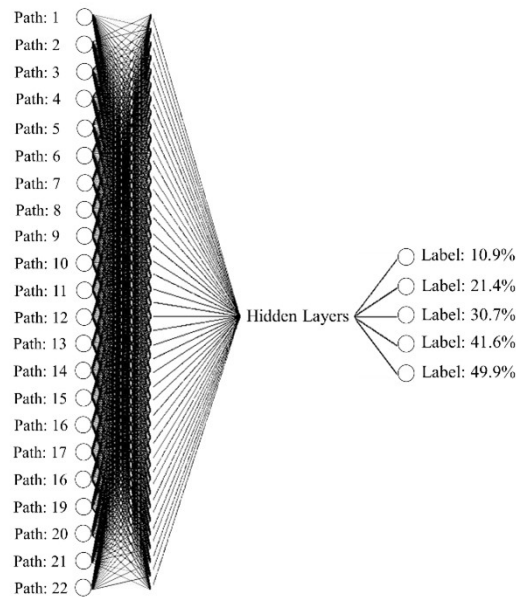

Figure 7. Architecture of ANN 2.

ANN 2 was trained with 5000 samples, i.e., 1000 samples for each label, and the training was evaluated from 100 new samples. Table 3 shows the network performance for the samples against the number of training epochs.

Table 3. ANN 2 training evaluation.

Epochs	Accuracy (%)
10	65
50	92
100	82
1000	91

It was noted that a higher number of epochs did not contribute to accuracy gains, so the number of 1000 epochs was set as the optimal number for ANN 2.

2.2.3 Architecture of ANN 3

The data format was also modified for the third architecture - instead of five labels, 18 different contents were covered. This is the maximum number of discretizations for the 100×200 mm^2 geometry, assuming each aggregate has 391.87 mm^2. Therefore, all possible contents were included in this new database.

ANN 1 and ANN 2 solved classification problems, and ANN 3 was conceived for regression problems. The 22 measurement paths required 22 neurons in the input layer. Four hidden layers with 128, 256, 256, 256 neurons were used, whereas only one was adopted for the output layer. *ReLU* was used for all hidden layers, and the *Linear* activation function was employed for the output layer. Figure 8 illustrates the ANN 3 architecture.
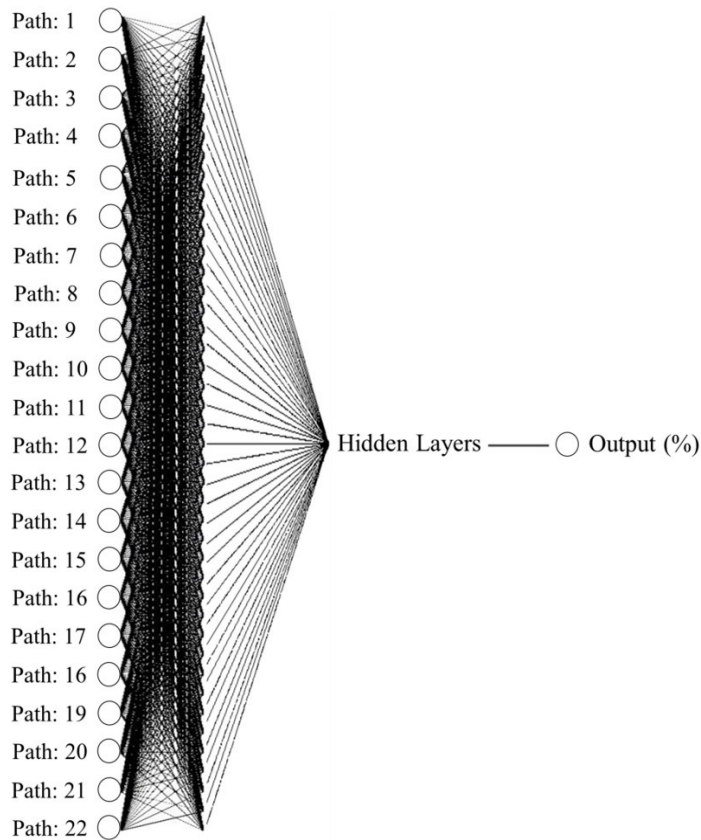
Rev. IBRACON Estrut. Mater., vol. 17, no. 6, e17612, 2024

10/21

Figure 8. Architecture of ANN 3.

Table 4 shows the relationship between the number of particles and coarse aggregate content.

Table 4. Coarse aggregate contents for the regression problem.

Specimen area (mm²)	Coarse aggregate area (mm²)	Number of coarse aggregates	Coarse aggregate contents (%)
		0	0.0
		1	2.0
		2	4.1
		3	6.2
		4	8.5
		5	10.9
		6	13.3
		7	15.9
		8	18.6
20000	391.87	9	21.4
		10	24.4
		11	27.5
		12	30.7
		13	34.2
		14	37.8
		15	41.6
		16	45.7
		17	49.9

Adam algorithm optimized the neural network, and the *Mean Absolute Error* (MAE) cost function Eq. (12) was used.

$$L(y, y^*) = \frac{\sum_{i=1}^{n} |y_i - y_i^*|}{n}$$

(12)

For the regression problem, the authors opted for evaluating the MAE instead of Accuracy because, in this case, it is not important to know how many times the algorithm hit the exact expected value. What matters in a regression problem is how close all solutions come to the expected response.

1000 samples were generated for each of the 18 coarse aggregate contents, thus leading to 18000 training samples.

The neural network was evaluated for a new data set with 18 contents by MAE associated with each training epoch. Table 5 shows the ANN 3 progress.

Table 5. ANN 3 training evaluation.

Epochs	MAE
10	0.02224
50	0.01796
100	0.02512
1000	0.01988
2000	0.01895

50 training epochs were set as an optimal number for ANN 3.

2.3 Error estimate between straight and non-straight paths

Straight path is a reasonable approach for heterogeneous media if the wave velocities do not vary more than 10% [56]. Therefore, the errors associated with straight paths in concrete structures must be assessed [20].

Dijkstra algorithm evaluated non-straight paths [57]; it calculates the shortest path using the total weight of the links between a starting node and all other nodes in a graph.

Therefore, the 100 x 200 mm^2 specimen was divided into 231 nodes (Figure 9). Links are small lines between nodes, and the weights at each link are proportional to the wave velocity.
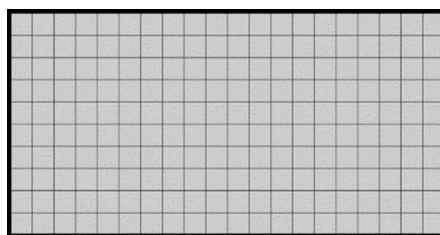

Figure 9. Specimen divided into 200 elements that form 231 nodes at their edges.

Figure 10 shows a sample used in the training of ANN 3 for the maximum coarse aggregate content (49.9%). The paths are supposed to be straight, and the coarse aggregates do not change their trajectory, but only their travel-time.
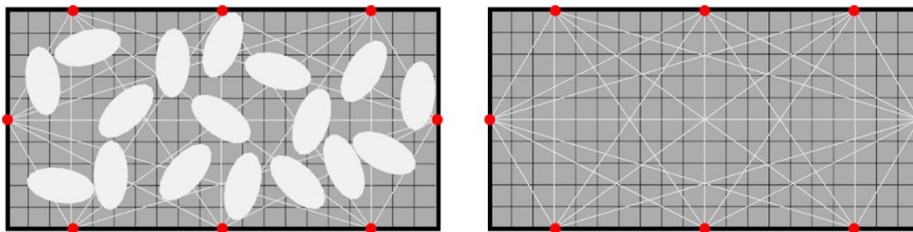
Rev. IBRACON Estrut. Mater., vol. 17, no. 6, e17612, 2024

12/21

Figure 10. Straight paths for 22 measurements at 49.9% coarse aggregate content.

However, Figure 11 displays the *paths updated* by Dijkstra. In this case, velocities and trajectories are modified.
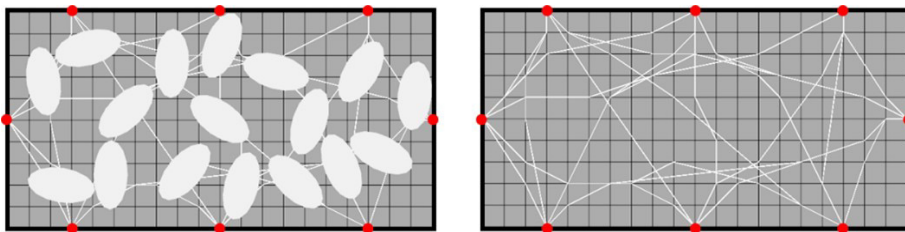

Figure 11. *Updated paths* for 22 measurements at 49.9% coarse aggregate content.

Artificial neural networks might also be trained with *updated paths*; however, such a choice would result in a high computational cost, since the training set is large.

The error associated with an ANN trained by straight paths can be estimated; it refers to the difference between the real coarse aggregate content and the ANN response when a set of *updated paths* is presented to the ANN. The importance of this analysis will be presented in section 3.4.

3 RESULTS

This section provides the results for the three neural networks and the error estimate for straight paths. A comparison among the performance of ANN 3 with other regression algorithms is also reported.

3.1 ANN 1 (13 paths): classification problem

ANN 1 has five output labels; however, since the contents may not coincide with the specified labels, a weighted average must be calculated between the output values. A new set with 80 samples was used with the following contents: 18.6%, 24.4%, 37.8%, and 45.7%. Figure 12 shows the absolute differences between the ANN 1 response and the real content.
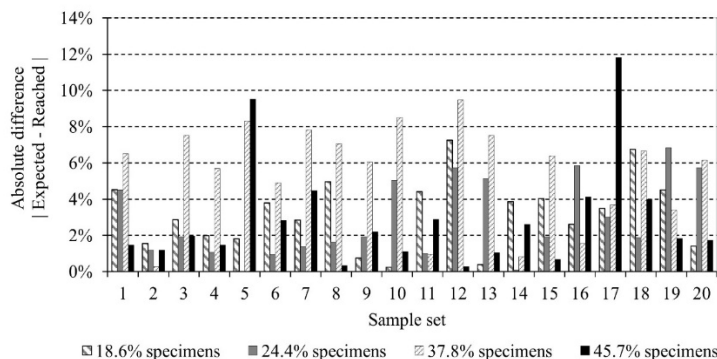

Figure 12. Absolute difference for ANN 1 in the samples with 18.6%, 18.6%, 24.4%, 37.8%, and 45.7% contents.

Only one sample showed an absolute deviation greater than 10% from the expected content. Table 6 shows the average, standard deviation, and coefficient of variation (CV) for each set of 20 samples.

Table 6. Global view of ANN 1 results.

Real content (%)	Average reached content (%)	Standard deviation (%)	CV (%)
18.6	21.09	2.76	13.1
24.4	25.44	3.39	13.3
37.8	40.43	5.50	13.6
45.7	44.42	3.85	8.67

The results of each sample and their average values demonstrate the good behavior of ANN 1.

As mentioned in section 2, the mortar was assigned a velocity of 3013 m/s and the coarse aggregates 5645 m/s. These values are consistent with those commonly found in experimental results.

Thus, Table 6 results indicate that the significant differences between the velocities of mortar and coarse aggregates allow the ANN to use them as recognition parameters.

3.2 ANN 2 (22 paths): classification problem

ANN 2 is expected to perform well for aggregates contents different than those used in training. Therefore, four sets of 20 specimens were generated with the following contents: 18.6%, 24.4%, 37.8%, 45.7%. Figure 13 shows the results.
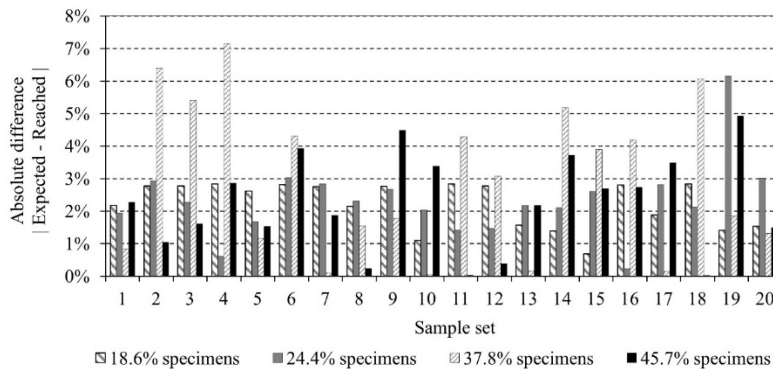

Figure 13. Absolute difference for ANN 2 in the samples with 18.6%, 18.6%, 24.4%, 37.8%, and 45.7% contents.

Only one out of the 80 samples evaluated showed an absolute deviation greater than 7%. Table 7 shows the average results.

Table 7. Global view of ANN 2 results.

Real content (%)	Average reached content (%)	Standard deviation (%)	CV (%)
18.6	20.28	1.62	7.99
24.4	23.48	2.42	10.3
37.8	38.37	3.68	9.59
45.7	44.41	2.33	5.25

According to the average results, ANN 2 performed slightly better than ANN 1, demonstrating an increase in the number of measurement paths that provides a neural network with a greater ability to identify the coarse aggregate content.

Rev. IBRACON Estrut. Mater., vol. 17, no. 6, e17612, 2024

14/21

3.3 ANN 3 (22 paths): regression problem

The performance of ANN 3 was compared with those of other regression methods, namely, *XGB Regressor*, *Random Forest*, and OLS (*Ordinary least squares*). The first two methods belong to XGBoost® and Scikit-Learn® libraries, and their basic parameters are shown in Table 8.

Table 8. Basic parameters for *XGB Regressor* and *Randon Forest*.

XGB Regressor		Randon Forest	
Booster	Tree base model	Number of trees in the forest	100
Number of gradients boosted trees	100	Minimum number of samples	2
Subsample ratio of columns (per tree, per level, per node)	1	Minimum number of samples to be a leaf node	1
Balance of positive and negative weights	1	Minimum weighted fraction	0
Importance type	*Gain*	Bootstrap samples are used	*True*
Maximum tree depth	3		
Minimum loss reduction (γ)	0		
L1 regularization (α)	0		
L2 regularization (λ)	1		
Learning rate (η)	0.1		
Minimum child weight	1		
Subsample ratio	1		
Initial prediction score	0.5		

Before presenting the results for the dataset intended for testing, it is worth mentioning the performance of the alternative methods for the training set. Table 9 shows the MAE values for them.

Table 9. *XGB Regressor, Random Forest,* and OLS training set performances.

Regression Method	MAE
ANN 3	0.01705
XGB Regressor	0.01082
Randon Forest	0.00883
OLS	0.02224

Thus, the fitting of data for all regression methods yielded results either close to or superior to ANN 3.

Initially, it is inferred that all analysis methods will serve the study's purposes, suggesting that the *XGB Regressor* and *Random Forest* might deliver superior results compared to ANN 3.

However, subsequent analyses will illustrate how these four methods can extend their solutions to a new dataset. This second approach will clarify the potential of ANN 3 in generalizing the problem.

The same data set used in the test of ANN 3 after training was applied for the assessment of the general performance of *XGB Regressor*, *Random Forest*, and OLS. Finally, Table 10 shows the results.

Table 10. *XGB Regressor*, *Random Forest,* and OLS testing set performances.

Regression Method	MAE
ANN 3	0.01796
XGB Regressor	0.02123
Random Forest	0.02348
OLS	0.02123

The average performance of ANN 3 was superior to those of the other methods. However, this global metric is not enough; for example, it suggests both OLS and *XGB Regressor* achieved the same performance, which is not true, as shown in the following analyses.

Another evaluation was conducted with 20 samples of each of the 18 contents. The results in Figure 14 correspond to the differences between the calculated average and the real content.
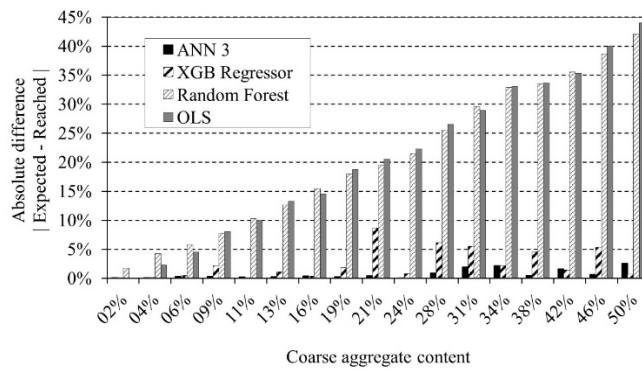
Rev. IBRACON Estrut. Mater., vol. 17, no. 6, e17612, 2024

15/21

Figure 14. Comparison between the regressions performed by ANN 3 and the regression algorithms evaluated: differences between sample averages and real content.

The performances of ANN 3 and *XGB Regressor* were superior to those of the other solutions, especially when assessing the highest contents.
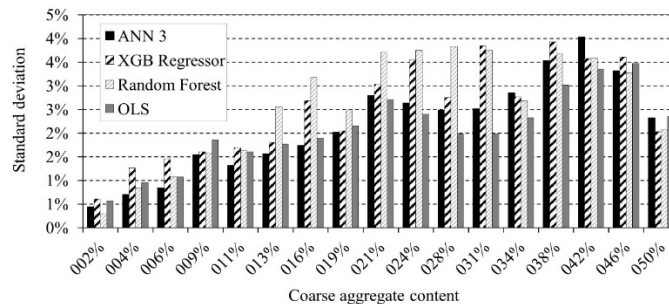
Figure 15 displays the standard deviation.

Figure 15. Comparison between the regressions performed by ANN 3 and the regression algorithms evaluated: standard deviation of sample averages.

Therefore, the regression provided by ANN 3 obtained a higher quality for the average values and a low standard deviation for all coarse aggregate contents.

ANN 1, ANN 2, and ANN 3 solutions were also compared for the contents of 18.6%, 24.4%, 37.8%, and 46.7%. Figure 16 shows the absolute difference between the average of the 20 samples evaluated by neural networks and the real content.
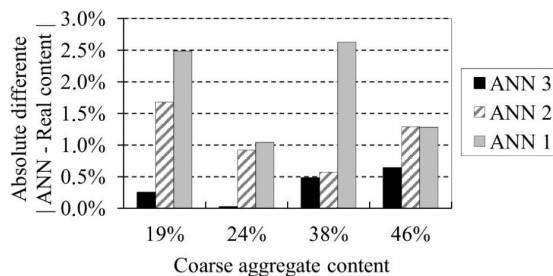

Figure 16. Comparison between ANNs´ performances.

As reported elsewhere, ANN 2 performed better than ANN 1. Therefore, the largest number of paths is an important variable for neural networks. ANN 3 obtained the best results in solving a regression problem.

3.4 Error estimate between straight and non-straight paths

As previously discussed, the calculations reported so far consider the paths to remain straight for a heterogeneous medium. This section reports the results for ANN 3, for which a sample with *updated paths* was used.

2.0%, 10.9%, 21.4%, 34.2%, 49.9% contents were chosen for the analysis. Figure 17 displays the ANN 3 response for straight paths and its response when initialized with *updated paths*. The *updated paths* were calculated by applying Dijkstra's algorithm as discussed in section 2.3.
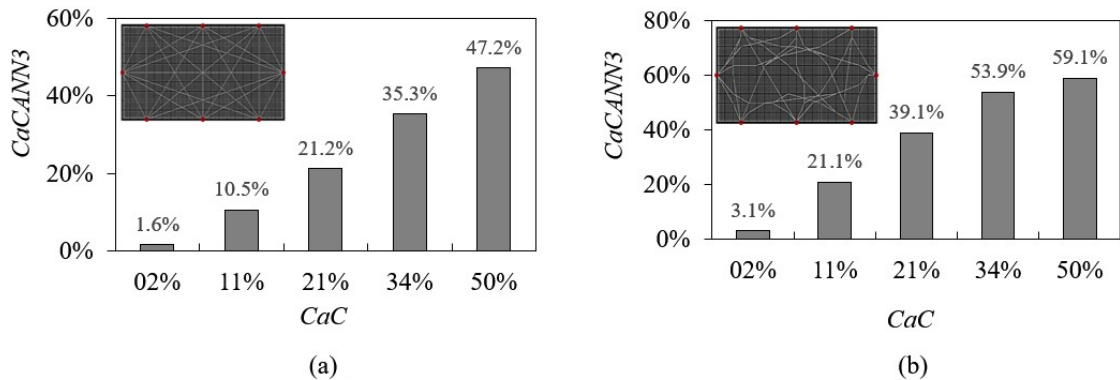

Figure 17. ANN 3 response for (a) straight paths and (b) *updated paths*.

An increase in the absolute difference between the real coarse aggregate content (*CaC*) and the ANN 3 response (*CaC$_{ANN3}$*) is clearly observed. However, it follows an approximately parabolic trend, as shown in Figure 18.
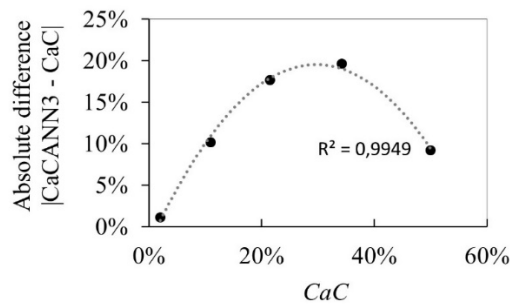

Figure 18. Parabolic trend for the error estimate between straight and non-straight paths.

The error decreases as the specimen resembles a continuous medium for low or high coarse aggregates´ contents.

Figure 18 displays a trendline that enables a correction for the ANN 3 responses. Equation 13 is valid for contents below 50% and represents the relationship between *CaC$_{ANN3}$* and its corrected value (*CaC**).

$$CaC^*\left(CaC_{ANN3}\right) = \begin{cases} 0.5 - 0.2034 \cdot \sqrt{5.837 - 9.833\left(CaC_{ANN3}\right)}, & \text{if } CaC_{ANN3} < 0.5 \\ 0.5, & \text{if } CaC_{ANN3} \geq 0.5 \end{cases} \tag{13}$$

A new data set of the five contents was generated to demonstrate the effectiveness of Equation 13. Table 11 shows the real coarse aggregate content, the ANN 3 response, and its corrected value.

Rev. IBRACON Estrut. Mater., vol. 17, no. 6, e17612, 2024

17/21

Table 11. Correction of the ANN3 response for updated paths.

Real coarse aggregate content (CaC)	ANN 3 response (CaC_{ANN3})	Corrected value (CaC^*)
2.0%	2.9%	2.1%
10.9%	20.6%	10.3%
21.4%	37.9%	20.4%
34.2%	52.6%	33.4%
49.9%	61.1%	50.0%

Equation 13 is not general and should be studied for each ANN architecture. However, due to the high computational costs involved in the generation of a database of *updated paths*, this approach may be convenient.

4 CONCLUSIONS AND FINAL REMARKS

This article proposed a strategy that combines artificial neural networks with the UPV technique to estimate the coarse aggregate content of concrete specimens.

Three neural network architectures were evaluated. The first two solved a classification problem, and the third resolved a regression one. The input data were the travel-time measured in UPV tests. ANNs with 13 (ANN 1) and 22 (ANN 2 and ANN 3) measurement paths were studied.

All approaches efficiently identified the coarse aggregate content. The best performance was obtained by ANN 3, which received 22 measurement paths and solved a regression problem.

ANN 3 was also evaluated against other regression techniques (*XGB Regressor*, *Random Forest*, and OLS) and showed superior performance.

An estimate of the error associated with the straight propagation paths, rather than *updated paths,* was assessed. The correction of results by the error estimate enables straight paths to be used as a training set, which results in a lower computational cost.

The satisfactory performance of the technique proposed has instigated further investigations. Therefore, after demonstrating the effectiveness of the proposed methodology, the next step of this research is dedicated to experimental evaluations.

The high number of measurements required for constructing paths and the heterogeneity present in the mortar pose a challenge. Nevertheless, these same challenges are also encountered in ultrasonic tomography techniques that have made significant advances. Thus, despite the novelty of the presented methodology, the authors believe that a productive area of inquiry has been opened.

5 ACKNOWLEDGMENTS

6 REFERENCES

[1]   B. S. Dhillon, *Life Cycle Costing for Engineers*, 1st ed. Boca Raton, FL: Taylor & Francis Group, 2010.

[2]   M. G. Grantham, *Concrete Repair: A Practical Guide*, 1st ed. Boca Raton, FL: CRC Press, 2011.

[3]   D. K. Panesar and S. E. Chidiac, "Ultrasonic pulse velocity for determining the early age properties of dry-cast concrete containing ground granulated blast-furnace slag," *Can. J. Civ. Eng.*, vol. 34, no. 5, pp. 682–385, May 2007, http://dx.doi.org/10.1139/l07-039.

[4]   G. Trtnik and M. Gams, "Ultrasonic assessment of initial compressive strength gain of cement based materials," *Cement Concr. Res.*, vol. 67, pp. 148–155, Jan 2015, http://dx.doi.org/10.1016/j.cemconres.2014.10.005.

[5]   S. Sharma and A. Mukherjee, "Monitoring freshly poured concrete using ultrasonic waves guided through reinforcing bars," *Cement Concr. Compos.*, vol. 55, pp. 337–347, Jan 2015, http://dx.doi.org/10.1016/j.cemconcomp.2014.09.011.

[6]   T. P. Philippidis and D. G. Aggelis, "An acousto-ultrasonic approach for the determination of water-to-cement ratio in concrete," *Cement Concr. Res.*, vol. 33, no. 4, pp. 525–538, Apr 2003, http://dx.doi.org/10.1016/S0008-8846(02)00999-7.

[7]   M. F. Kaplan, "The effects of age and water/cement ratio upon the relation between ultrasonic pulse velocity and compressive strength of concrete," *Mag. Concr. Res.*, vol. 11, no. 32, pp. 85–92, Jul 1959, http://dx.doi.org/10.1680/macr.1959.11.32.85.

Rev. IBRACON Estrut. Mater., vol. 17, no. 6, e17612, 2024

18/21

[8]   Y. Wang et al., "The effect of water-cement ratio on acousto-ultrasonic characteristics in mortar," *Russ. J. Nondestr. Test.*, vol. 53, pp. 148–158, May 2017, http://dx.doi.org/10.1134/S1061830917020097.

[9]   C. C. Ferraro, J. A. Boyd, and R. G. Consolazio, "Evaluation of damage to bridge piers using pulse velocity tomography," *Constr. Build. Mater.*, vol. 38, pp. 1303–1309, Jan 2013, http://dx.doi.org/10.1016/j.conbuildmat.2012.09.003.

[10] M. Nematzadeh and A. Baradaran-Nasiria, "Mechanical performance of fiber-reinforced recycled refractory brick concrete exposed to elevated temperatures," *Comput. Concr.*, vol. 24, no. 1, pp. 19–35, Jan 2019, http://dx.doi.org/10.12989/cac.2019.24.1.019.

[11] J. Yoon, H. Kim, S. W. Shin, and S. H. Sim, "Rheology-based determination of injectable grout fluidity for preplaced aggregate concrete using ultrasonic tomography," *Constr. Build. Mater.*, vol. 260, pp. 120447, Nov 2020, http://dx.doi.org/10.1016/j.conbuildmat.2020.120447.

[12] C. Colombero, C. Comina, A. Giuliani, and G. Mandrone, "Ultrasonic equipment aimed to detect grouting homogeneity in geothermal heat exchangers", in *Proceedings of European Geothermal Congress* (Strasbourg, France), Sep. 2016. iris.unito.it/bitstream/2318/1602270/1/77_16.pdf (accessed Aug. 17, 2023).

[13] I. Lillamand, J. F. Chaix, M. A. Ploix, and V. Garnier, "Acoustoelastic effect in concrete material under uni-axial compressive loading," *NDT Int.*, vol. 43, no. 8, pp. 655–660, Nov 2010, http://dx.doi.org/10.1016/j.ndteint.2010.07.001.

[14] K. F. Bompan and V. G. Haach, "Ultrasonic tests in the evaluation of the stress level in concrete prisms based on the acoustoelasticity," *Constr. Build. Mater.*, vol. 162, pp. 740–750, Feb 2018, http://dx.doi.org/10.1016/j.conbuildmat.2017.11.153.

[15] S. C. Stähler, C. Sens-Schönfelder, and E. Niederleithinger, "Monitoring stress changes in a concrete bridge with coda wave interferometry," *J. Acoust. Soc. Am.*, vol. 129, no. 4, pp. 1945–1952, Apr 2011, http://dx.doi.org/10.1121/1.3553226.

[16] R. M. L. Gondim and V. G. Haach, "Monitoring of ultrasonic velocity in concrete specimens during compressive loading-unloading cycles," *Constr. Build. Mater.*, vol. 302, pp. 124218, Oct 2021, http://dx.doi.org/10.1016/j.conbuildmat.2021.124218.

[17] V. G. Haach and F. C. Ramirez, "Qualitative assessment of concrete by ultrasound tomography," *Constr. Build. Mater.*, vol. 119, pp. 61–70, Aug 2016, http://dx.doi.org/10.1016/j.conbuildmat.2016.05.056.

[18] M. Zielińska and M. Rucka, "Non-destructive assessment of masonry pillars using ultrasonic tomography," *Materials (Basel)*, vol. 11, no. 12, pp. 2543, Dec 2018, http://dx.doi.org/10.3390/ma11122543.

[19] L. P. Perlin, R. C. A. Pinto, and Â. Valle, "Ultrasonic tomography in wood with anisotropy consideration," *Constr. Build. Mater.*, vol. 229, pp. 116958, Dec 2019, http://dx.doi.org/10.1016/j.conbuildmat.2019.116958.

[20] L. P. Perlin and R. C. A. Pinto, "Use of network theory to improve the ultrasonic tomography in concrete," *Ultrasonics*, vol. 96, pp. 185–195, Jul 2019, http://dx.doi.org/10.1016/j.ultras.2019.01.007.

[21] M. Zielińska and M. Rucka, "Detection of debonding in reinforced concrete beams using ultrasonic transmission tomography and hybrid ray tracing technique," *Constr. Build. Mater.*, vol. 262, pp. 120104, Nov 2020, http://dx.doi.org/10.1016/j.conbuildmat.2020.120104.

[22] D. Camassa, A. Castellano, A. Fraddosio, and M. D. Piccioni, "A new ultrasonic amplitude tomography approach, with validation on masonry tuff blocks," *J. Nondestr. Eval.*, vol. 39, no. 3, pp. 1–19, Jun 2020, http://dx.doi.org/10.1007/s10921-020-00693-2.

[23] D. P. Dos Santos and V. G. Haach, "Generation of ultrasonic tomography from time-domain propagation spectrum," *Ultrasonics*, vol. 120, pp. 106666, Mar 2022, http://dx.doi.org/10.1016/j.ultras.2021.106666.

[24] M. A. P. Irrigaray, R. C. A. Pinto, and I. J. Padaratz, "A new approach to estimate compressive strength of concrete by the UPV method," *Rev. IBRACON Estrut. Mater.*, vol. 09, no. 03, pp. 395–402, Jun 2016, http://dx.doi.org/10.1590/S1983-41952016000300004.

[25] S. T. Martins et al., "Characterization of pervious concrete focusing on non-destructive testing," *Rev. IBRACON Estrut. Mater.*, vol. 13, no. 03, pp. 483–500, May-Jun 2020, http://dx.doi.org/10.1590/S1983-41952020000300003.

[26] K. Haddad et al., "Correlation between the porosity and ultrasonic pulse velocity of recycled aggregate concrete at different saturation levels," *Can. J. Civ. Eng.*, vol. 44, no. 11, pp. 911–917, Jun 2017, http://dx.doi.org/10.1139/cjce-2016-0449.

[27] M. Nematzadeh, R. Poorhosein, "Estimating properties of reactive powder concrete containing hybrid fibers using UPV," *Comput. Concr.*, vol. 20, no. 4, pp. 491–502, Oct 2017, http://dx.doi.org/10.12989/cac.2017.20.4.491.

[28] C. Wang, H. Wang, S. Chang, "Prediction models of compressive strength and UPV of recycled material cement mortar," *Comput. Concr.*, vol. 19, no. 4, pp. 419–427, Jan 2017, http://dx.doi.org/10.12989/cac.2017.19.4.419.

[29] A. Adesina, J. Cercel, and S. Das, "Effect of curing conditions on the compressive strength of sodium carbonate activated slag–glass powder mortar," *Can. J. Civ. Eng.*, vol. 48, no. 8, pp. 1056–1061, Sep 2020, http://dx.doi.org/10.1139/cjce-2020-0065.

[30] L. P. Perlin, R. C. Andrade Pinto, and Â. Valle "Ultrasonic tomography in wood with anisotropy consideration," *Construction Build. Mater.*, vol. 229, no. 2019, pp. 116958, Dec. 2019, https://doi.org/10.1016/j.conbuildmat.2019.116958.

[31] L. P. Perlin, Â. Valle, and R. C. Andrade Pinto, "New method to locate the pith position in a wood cross-section based on ultrasonic measurements," *Constr. Build. Mater.*, vol. 169, pp. 733–739, Apr 2018., http://dx.doi.org/10.1016/j.conbuildmat.2018.03.021.

[32] F. J. Pallarés, M. Betti, G. Bartoli, and L. Pallarés, "Structural health monitoring (SHM) and Nondestructive testing (NDT) of slender masonry structures: a practical review," *Constr. Build. Mater.*, vol. 297, pp. 123768, Aug 2021., http://dx.doi.org/10.1016/j.conbuildmat.2021.123768.

[33] D. Camassa, A. Castellano, A. Fraddosio, and M. D. Piccioni, "A new ultrasonic amplitude tomography approach, with validation on masonry tuff blocks," *J. Nondestr. Eval.*, vol. 39, no. 3, pp. 1–19, Oct 2019, http://dx.doi.org/10.1007/s10921-020-00693-2.

[34] F. J. Tallavo, M. D. Pandey, G. Cascante, and C. A. Lara, "Ultrasonic and acoustic pulse velocity methods for nondestructive detection of early decay in wood poles," *Can. J. Civ. Eng.*, vol. 49, no. 6, pp. 1059–1068, Oct 2021, http://dx.doi.org/10.1139/cjce-2020-0658.

[35] A. Lorenzi, J. Campagnolo, and L. C. P. Silva Fo., "Application of artificial neural network for interpreting ultrasonic readings of concrete," *Int. J. Mater. Prod. Technol.*, vol. 26, no. 1-2, pp. 57–70, Feb 2006, http://dx.doi.org/10.1504/IJMPT.2006.008980.

[36] I. B. Topcu and M. Sarıdemir, "Prediction of properties of waste AAC aggregate concrete using artificial neural network," *Comput. Mater. Sci.*, vol. 41, no. 1, pp. 117–125, Nov 2007, http://dx.doi.org/10.1016/j.commatsci.2007.03.010.

[37] J. Ongpeng, M. Soberano, A. Oreta, and S. Hirose, "Artificial neural network model using ultrasonic test results to predict compressive stress in concrete," *Comput. Concr.*, vol. 19, no. 1, pp. 59–68, Jan 2017, http://dx.doi.org/10.12989/cac.2017.19.1.059.

[38] A. M. Tahwia, A. Heniegal, M. S. Elgamal, and B. A. Tayeh, "The prediction of compressive strength and non-destructive tests of sustainable concrete by using artificial neural networks," *Comput. Concr.*, vol. 27, no. 1, pp. 21–28, Dec 2020, http://dx.doi.org/10.12989/cac.2021.27.1.021.

[39] M. Bilgehan and P. Turgut, "Artificial neural network approach to predict compressive strength of concrete through ultrasonic pulse velocity," *Res. Nondestruct. Eval.*, vol. 21, no. 1, pp. 1–17, Jan 2010, http://dx.doi.org/10.1080/09349840903122042.

[40] R. Madandoust, R. Ghavidel, and N. Nariman-Zadeh, "Evolutionary design of generalized GMDH-type neural network for prediction of concrete compressive strength using UPV," *Comput. Mater. Sci.*, vol. 49, no. 3, pp. 556–567, Sep 2010, http://dx.doi.org/10.1016/j.commatsci.2010.05.050.

[41] A. Lorenzi, L. C. P. Silva Fo., and J. L. Campagnolo, "Desenvolvimento de redes neurais artificiais para interpretação de ensaios de velocidade de propagação de pulso ultrassônico no concreto," *Rev. IBRACON Estrut. Mater.*, vol. 4, no. 5, pp. 829–844, Dec 2011, http://dx.doi.org/10.1590/S1983-41952011000500008.

[42] A. A. Shah, S. H. Alsayed, H. Abbas, and Y. A. Al-Salloum, "Predicting residual strength of non-linear ultrasonically evaluated damaged concrete using artificial neural network," *Constr. Build. Mater.*, vol. 29, pp. 42–50, Apr 2012, http://dx.doi.org/10.1016/j.conbuildmat.2011.10.038.

[43] Y. Xu and R. Jin, "Measurement of reinforcement corrosion in concrete adopting ultrasonic tests and artificial neural network," *Constr. Build. Mater.*, vol. 177, pp. 125–133, Jul 2018, http://dx.doi.org/10.1016/j.conbuildmat.2018.05.124.

[44] A. J. Tenza-Abril, Y. Villacampa, A. M. Solak, and F. Baeza-Brotons, "Prediction and sensitivity analysis of compressive strength in segregated lightweight concrete based on artificial neural network using ultrasonic pulse velocity," *Constr. Build. Mater.*, vol. 189, pp. 1173–1183, Nov 2018, http://dx.doi.org/10.1016/j.conbuildmat.2018.09.096.

[45] A. Jain, S. K. Jha, and S. Misra, "Modeling and analysis of concrete slump using artificial neural networks," *J. Mater. Civ. Eng.*, vol. 20, no. 9, pp. 628–633, Sep 2008, http://dx.doi.org/10.1061/(ASCE)0899-1561(2008)20:9(628).

[46] E. Ghafari, M. Bandarabadi, H. Costa, and E. Júlio, "Prediction of fresh and hardened state properties of UHPC: comparative study of statistical mixture design and an artificial neural network model," *J. Mater. Civ. Eng.*, vol. 27, no. 11, pp. 04015017, Feb 2015, http://dx.doi.org/10.1061/(ASCE)MT.1943-5533.0001270.

[47] M. N. Soutsos, J. H. Bungey, S. G. Millard, M. R. Shaw, and A. Patterson, "Dielectric properties of concrete and their influence on radar testing," *NDT Int.*, vol. 34, no. 6, pp. 419–425, Sep 2001, http://dx.doi.org/10.1016/S0963-8695(01)00009-3.

[48] X. Dérobert and G. Villain, "Development of a multi-linear quadratic experimental design for the EM characterization of concretes in the radar frequency-band," *Constr. Build. Mater.*, vol. 136, pp. 237–245, Apr 2017, http://dx.doi.org/10.1016/j.conbuildmat.2016.12.061.

[49] G. Villain, A. Ihamouten, and X. Derobert, "Determination of concrete water content by coupling electromagnetic methods: Coaxial/cylindrical transition line with capacitive probes," *NDT Int.*, vol. 88, pp. 59–70, Jun 2017, http://dx.doi.org/10.1016/j.ndteint.2017.02.004.

[50] K. J. Bois, A. D. Benally, and R. Zoughi, "Microwave near-field reflection property analysis of concrete for material content determination," *IEEE Trans. Instrum. Meas.*, vol. 49, no. 1, pp. 49–55, Jan 2000., http://dx.doi.org/10.1109/19.836308.

[51] P. K. Mehta and P. J. M. Monteiro, *Concrete: Microstructure, Properties, and Materials*, 3rd ed. New York: McGraw-Hill, 2006.

[52] International Atomic Energy Agency, *Guidebook on Non-Destructive Testing of Concrete Structures* (Training Course Series, 17). Vienna, Austria: IAEA, 2002.

[53] H. W. Chung and K. S. Law, "Diagnosing in situ concrete by ultrasonic pulse technique," *Chem. Int.*, vol. 5, no. 10, pp. 42–49, Jan 1983. concrete.org/publications/internationalconcreteabstractsportal/m/details/id/9183 (accessed Aug. 17, 2023).

[54] I. Palomar and G. Barluenga, "Assessment of lime-cement mortar microstructure and properties by P- and S-ultrasonic waves," *Constr. Build. Mater.*, vol. 139, pp. 334–341, May 2017, http://dx.doi.org/10.1016/j.conbuildmat.2017.02.083.

[55] D. P. Kingma, J. Ba, "Adam: A method for stochastic optimization," *arXiv*, Dec. 2014, https://doi.org/10.48550/arXiv.1412.6980

[56] M. J. Jackson and D. R. Tweeton, *MIGRATOM: Geophysical Tomography Using Wavefront Migration and Fuzzy Constraints* (Technical report). Wasinghton, USA: U.S. Department of Interior – Bureau of Mines, 1994.

[57] E. W. Dijkstra, "A note on two problems in connexion with graphs," *Numer. Math.*, vol. 1, no. 1, pp. 269–271, Jun 1959., http://dx.doi.org/10.1007/BF01386390.

Rev. IBRACON Estrut. Mater., vol. 17, no. 6, e17612, 2024

21/21